JOURNAL OF MATERIALS SCIENCE **34** (1999) 3405–3412

Mechanical behavior of SiC fiber reinforced brittle-matrix composites

T. OKABE*, J. KOMOTORI, M. SHIMIZU
Department of Mechanical Engineering, Keio University, 3-14-1 Hiyoshi, Kohoku-ku, Yokohama 223-8522, Japan
E-mail: tomonaga@compmat.rcast.u-tokyo.ac.jp

N. TAKEDA
Center for Collaborative Research (CCR), The University of Tokyo, 4-6-1 Komaba, Meguro-ku, Tokyo 153-8904, Japan

The failure process of unidirectional BN-coated HI-NICALON^{TM} SiC fiber reinforced glass matrix composites was examined under tensile loading. *In situ* observation of the mean matrix crack interval was conducted by the replica observation during tensile testing. Axisymmetric cylindrical models extended to the system considering the strength distribution of fibers were proposed to predict the whole stress-strain curve for comparison with the experimental results.

1. Introduction

It is now well known that failure modes in continuous fiber-reinforced ceramic matrix composites (CMC) involve initial and multiple matrix cracks, since the matrix has a lower failure strain than fibers. Then, fiber/matrix debondings occur from the tip of matrix cracks due to weak fiber/matrix interfaces (Fig. 1), so that fibers can bridge the crack and support further loads before the final fracture. Therefore, the optimization of interfacial design is necessary for the structural reliability of CMC [1–3].

Many analyses have been proposed to characterize the damage progress in CMC, considering the "weak" interfaces [4, 5]. Hutchinson and Jensen [5] used axisymmetric cylindrical models for stress analysis in CMC and quantitatively showed the effects of the interfacial debonding and sliding friction on the matrix cracking. Marshall [6] examined the use of Hutchinson and Jensen's analysis to deduce interfacial properties from experimental measurements of fiber sliding and provided explicit relations for the relative displacement as a function of increasing applied stress.

Most approaches for measuring mechanical properties of interfaces have used micro-model tests [7], including pushing and pulling of fibers. In such micro-model tests, it is difficult to reproduce the micro-mechanical damage in real composites, which has a wide variety of damage stages including matrix crack, debonding and fiber failure. Then, to estimate the micro-mechanical damage in real composites, the prediction of the stress-strain curve is considered to be attractive. This analysis can provide a quantitative estimation of not only the micro-mechanical damage but also the mechanical properties of interfaces. Vagaggini *et al.* [8] proposed a model for the prediction of the stress-strain curve for the composites with multiple matrix cracks, using Hutchinson and Jensen's analysis.

The interfacial properties also influence the damage progress after matrix cracks are saturated [9, 10]. Curtin [10] proposed a model for the ultimate tensile strength prediction considering both bridging and pull-out forces of fibers, and showed that the theory had a good agreement with experimental data. Since these studies are based on the theory of the ideal single fiber composites, the conditions of interfacial behavior (such as debonding) for the composites are neglected. Thus a new model should be constructed to connect interfacial properties with the behavior of fibers. To this end, more experimental supports are necessary to quantify the micro-mechanical damage progress.

The objective of the present study is to experimentally examine the tensile damage growth process in unidirectional BN-coated HI-NICALON^{TM} SiC fiber reinforced glass matrix composites, and to compare the experimental results with the theoretical predictions based on a new model which considers matrix cracking, debonding, and fiber strength distribution.

The remainder of this paper is structured as follows: In Section 2 experimental procedures are described. In Section 3 a new model is described for the prediction of the stress-strain curve. In Section 4 experimental results are shown. In Section 5 comparison of theoretical and experimental results are presented. And further discussion is conducted.

2. Experiments

HI-NICALON^{TM} (Nippon Carbon Co. Ltd.) is an improved high-temperature SiC fiber with low-oxygen content. Two types of HI-NICALON^{TM} fibers were

* Author to whom all correspondence should be addressed.

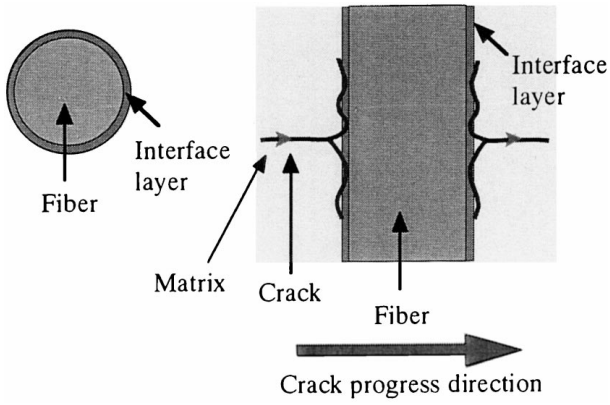

Figure 1 Schematic of crack deflection.

used to fabricate unidirectional fiber reinforced borosilicate glass (PYREX^{TM}) matrix composites: (1) fibers without coating, and (2) fibers CVD-coated with 1 μm-thick BN. Prepregs were prepared by a glass slurry method and hot-pressed at 1000 °C for 60 minutes, to fabricate 100 × 100 × 2.5 mm plates.

Tensile test specimens with dimensions of 100 × 3 × 2.5 mm were cut from the fabricated plates and tapered GFRP tabs were glued at both sides to provide a gauge length of 30 mm. Tensile tests were performed at a constant cross-head speed of 0.4 mm/min at room temperature in air. A computer-assisted data acquisition system was used to obtain the stress-strain curves from a strain gage placed on the specimen and a load cell. The specimen surfaces were polished with fine diamond pastes. Loaded specimens were periodically stopped under tension to replicate the damage progress on specimen surfaces using polyacetate films. This technique provides the *in situ* damage monitoring and the quantitative measurement of the matrix crack spacing or density.

In-situ fiber strength is expected to decrease due to degradation during the high-temperature fabrication. So, the *in-situ* fiber strength data were obtained by single fiber tension tests (gage length = 25 mm) using fibers extracted from fabricated plates. The fabricated plates were dipped into acid solutions for 3 days to dissolve the glass matrix, washed in water, and then dried in air to obtain extracted fibers.

3. Analysis

3.1. Axisymmetric cylindrical models with two matrix cracks

The analysis of stress and strain distribution near a matrix crack with fiber/matrix debonding is necessary to establish a model for the damage initiation and growth behavior with the interfacial properties. Hutchinson and Jensen [5] proposed an axisymmetric cylindrical model for a single matrix crack in an infinite body, using a Lamé problem. In this paper, the analysis is extended for a new model with two matrix cracks, which represents a general model for multiple matrix cracks (Fig. 2). Although the expression of Hutchinson and Jensen is appropriate for stress and strain distribution near a matrix crack, their analysis does not consider the fiber

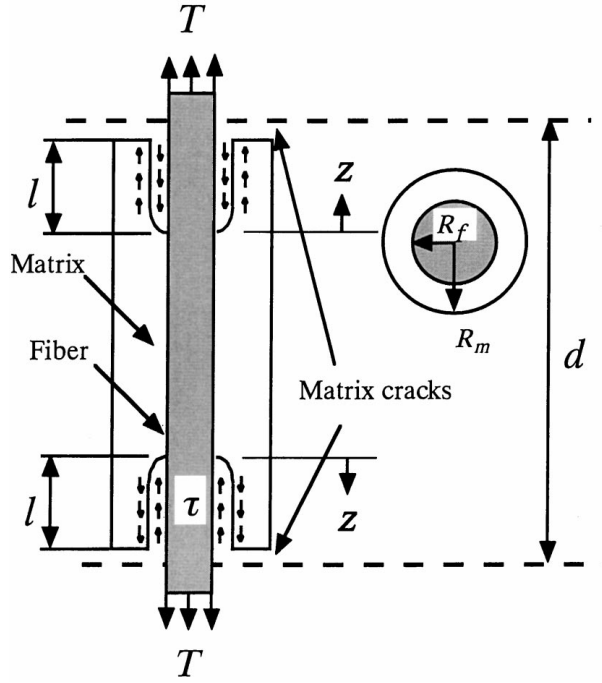

Figure 2 Axisymmetric cylindrical cell model.

strength distribution. In order to consider fiber failure, the present analysis is used under the condition that the axial fiber stress is given by T at the matrix crack plane. T is given as a function of the overall stress σ (In Section 3.4). Marshall [6] modified the expression given by Hutchinson and Jensen, using T. In this paper, Marshall's expression is used to explain a model.

The present model forms a repeating unit of a unidirectional composite with a fiber volume fraction $V_f = (R_f/R_m)^2$, and consists of debonded (length l from both matrix cracks) and bonded regions. Here, the matrix crack spacing is d, and the sliding stress is τ. Although Hutchinson and Jensen give solutions for fibers which are anisotropic, the present analysis assumes that fibers are isotropic.

In the bonded region (denoted by a superscript (+)), the stresses and strains are given by solving a Lamé problem as,

$$\sigma_f^+ = a_1 V_f T - a_2 E_m \varepsilon_z^T \quad (1)$$

$$\varepsilon_f^+ = a_5 (V_f T / E_m) + a_6 \varepsilon_z^T \quad (2)$$

$$\sigma_m^+ = (E_m/E_c) V_f T + \frac{V_f}{1 - V_f} a_2 E_m \varepsilon_z^T \quad (3)$$

$$\varepsilon_z^T = \int_0^{\Delta T} (\alpha_f - \alpha_m)\, dt \quad (4)$$

where ε_z^T is a residual strain due to the thermal expansion mismatch between a fiber and matrix, a_1–a_6 are non-dimensional parameters given by Hutchinson and Jensen [5], and shown in Table I. The subscripts f, m, and c denote fibers, matrix and composites, respectively. E and α are Young's modulus and thermal expansion coefficient, respectively. ΔT is a difference in tested and fabricated temperatures.

In the debonded region, the differences in stresses and strains relative to those in the bonded region (i.e.

TABLE I Summary of constants

$a_1 = \dfrac{E_f}{E_c}$	$b_1 = \dfrac{\{(1-\nu^2)E^* + (1-\nu)^2 E_m - (1+\nu)[2(1-\nu)^2 E_f + (1-2\nu)(1-\nu+V_f(1+\nu))(E_m - E_f)]\}}{2\nu(1-\nu)[(1+\nu)E^* + (1-\nu)E_m]}$
$a_2 = \dfrac{(1-V_f)(1+\nu+(1+\nu)(E_f/E_c))}{(1+\nu)(E_f+(1-2\nu)E_c)}$	$b_2 = \dfrac{(1+\nu)E_m\{2(1-\nu)^2 E_f + (1-2\nu)[1-\nu+V_f(1+\nu)](E_m - E_f)\}}{(1-\nu)E_f[(1+\nu)E^* + (1-\nu)E_m]}$
$a_3 = 0$	$b_3 = \dfrac{V_f(1+\nu)\{(1-V_f)(1+\nu)(1-2\nu)(E_f - E_m) + 2(1-\nu)^2 E_m\}}{(1-\nu)(1-V_f)[(1+\nu)E^* + (1-\nu)E_m]}$
$a_4 = \dfrac{(1-V_f)(1+\nu)E_f}{(1+\nu)(E_f+(1-2\nu)E_c)}$	$c_1 = \dfrac{(1-V_f a_1)(b_2+b_3)^{1/2}}{2V_f}$
$a_5 = \dfrac{E_m}{E_c}$	$c_2 = \dfrac{a_2(b_2+b_3)^{1/2}}{2}$
$a_5 = V_f \dfrac{E_f}{E_c}$	$c_3 = \dfrac{E_c}{E_m}$
$E_c = V_f E_f + (1-V_f)E_m$	
$E^* = (1-V_f)E_f + V_f E_m$	

$\Delta\sigma_f = \sigma_f - \sigma_f^+$, $\Delta\varepsilon_f = \varepsilon_f - \varepsilon_f^+$,) are also given by solving a Lamé problem.

$$\Delta\sigma_m = -\frac{V_f}{1-V_f}\Delta\sigma_f \tag{5}$$

$$\Delta\varepsilon_f = b_2\Delta\sigma_f/E_m \tag{6}$$

$$\Delta\varepsilon_m = -b_3\Delta\sigma_f/E_m \tag{7}$$

where b_1–b_3 (Table I) are also non-dimensional parameters (Type 2 condition) given by Hutchinson and Jensen [5]. Their analysis provides two boundary conditions. Marshall [6] discussed how these parameters alter by change of mechanical properties and reported the difference of these conditions. The Type 1 condition is appropriate for a single fiber in matrix, such as pull-out or push-out experiments. The Type 2 condition is appropriate for composites where all the fibers are bridging a matrix crack. Therefore, the present analysis is used only for the Type 2 condition. If, for simplicity, the constant sliding stress τ is assumed to act on all debonded surfaces, the axial fiber stress in the debonded region is given by solving a shear-lag problem with Equation 8

$$\sigma_f = T - 2\tau\frac{l-z}{R_f} \tag{8}$$

This stress distribution, as well as Hutchinson and Jensen's one, has a large gap γ at a debonding crack tip (Fig. 3). This gap can be written in terms of the Mode II

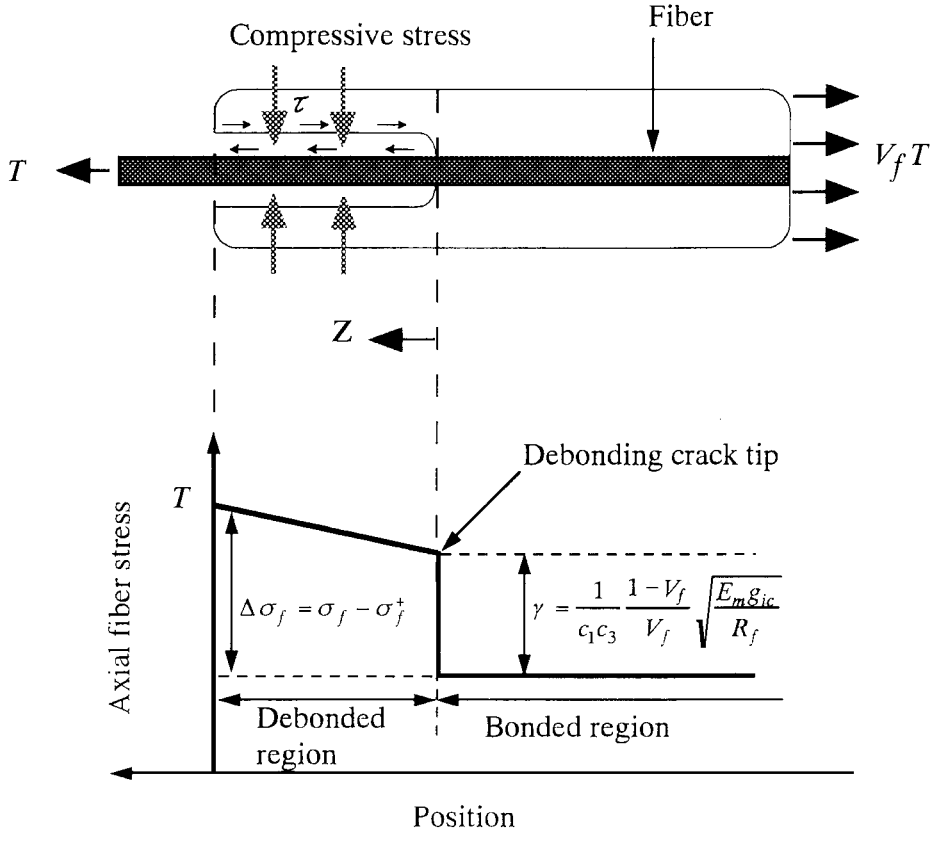

Figure 3 Axial fiber stress distribution.

interfacial fracture toughness g_{ic} and non-dimensional parameters c_1 and c_3 (Table I).

$$\gamma = \frac{1}{c_1 c_3} \frac{1 - V_f}{V_f} \sqrt{\frac{E_m g_{ic}}{R_f}} \tag{9}$$

3.2. Average matrix crack spacing

As the applied stress increases, more matrix cracks are generated between existing cracks, which are called multiple matrix cracks. Debonding always occurs at the tip of matrix cracks in CMC, when matrix cracks are generated in the composites. The length of debonding also increases as the applied stress increases [11]. As the neighboring debondings are connected, matrix cracks tend to be saturated. Therefore, the matrix crack interval depends on the debonding length. Curtin [10] proposed an exact theory for them with the sliding length, which is equal to the debonding length ($g_{ic} = 0$ N m^{-1}). However, the theory requires a very complicated numerical approach which considers the distribution of the matrix crack interval. The present analysis, for simplicity, uses the Weibull expression for matrix cracks. Similar to Curtin's approach, this model assumes that matrix cracks are generated in bonded regions.

If each matrix crack is assumed to have a gauge length as long as the final matrix crack spacing d_s (shown in Fig. 4), the probability of failure for matrix cracks in the composites is given by

$$P_f = 1 - \exp\left\{-\left(\frac{\sigma_m^+ - \sigma_{mu}}{\sigma_{m0}}\right)^{\bar{m}}\right\} \tag{10}$$

where σ_{m0} is a scale parameter, $\bar{m}$ is a Weibull modulus and σ_{mu} is the stress level as the first matrix crack occurs. The average matrix spacing d is given by using d_s.

$$d = \frac{L}{\left(\frac{L}{d_s} - 1\right) P_f} \cong \frac{d_s}{P_f} \tag{11}$$

Here for low density ($\frac{\sigma_m^+ - \sigma_{mu}}{\sigma_{m0}} \ll 1$), Equation 11 can be converted to Equation 12

$$d = d_s \left(\frac{E_c \sigma_{m0}}{E_m V_f (T - T_{mu})}\right)^{\bar{m}} \tag{12}$$

where T_{mu} is the axial fiber stress at the matrix crack plane when the first matrix crack occurs. Then, Equation 12 is the almost same expression as given by Vagaggini *et al.* [8] at $\bar{m} = 1$.

3.3. Debonding length

The stress and strain distribution depends on the debonding length. Considering both sliding stress and Mode II fracture toughness, the debonding length l is given by

$$\frac{l}{R_f} = \frac{1 - V_f}{V_f} (V_f T - \sigma_i)/2c_3\tau \tag{13}$$

where σ_i is a function of g_{ic}, given by Hutchinson and Jensen [5]. After l attains a half of the final matrix crack spacing ($d_s/2$), l is, for simplicity, assumed to be equal to ($d_s/2$).

3.4. Axial fiber stress at the matrix crack plane

After matrix cracks are saturated, only fibers can carry most of the applied stress in the composites.

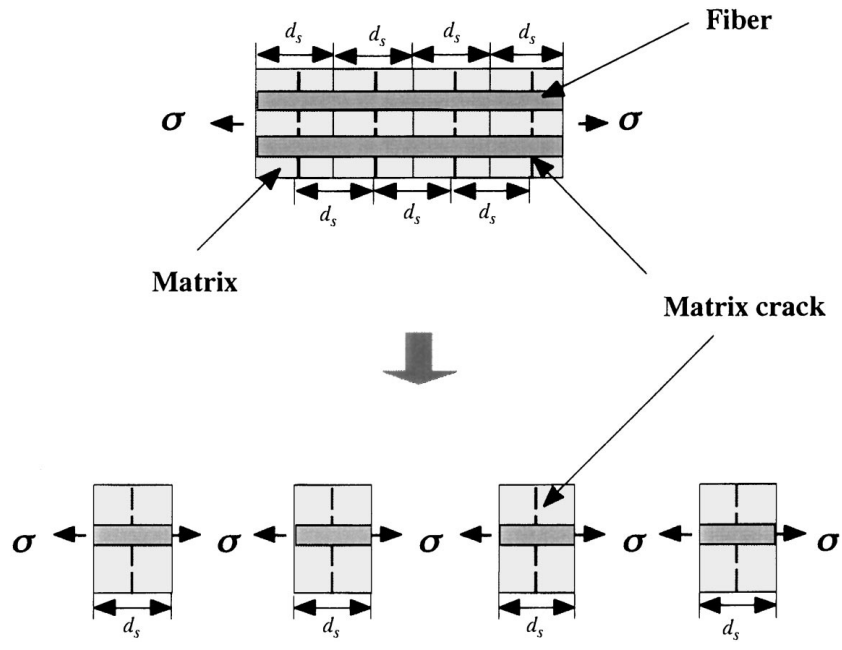

Figure 4 Matrix crack evolution.

The mechanical behavior, then, depends on the fiber strength. Curtin [10] discussed how the fiber stress is related with both the fiber strength distribution and the sliding stress. In the present model, the fiber stress T at the matrix crack plane is assumed to be that given by the Curtin model [10].

The Curtin model assumes that the force equilibrium equation at the matrix crack plane is given by

$$\frac{\sigma}{V_f} = (1 - P_f(2l_f, T))T + \frac{2\tau}{R_f}\langle L\rangle P_f(2l_f, T) \quad (14)$$

where $l_f\,(= R_f T/2\tau)$ is the effective pullout length, $\langle L\rangle$ the average pullout length, and $P_f(2l_f, T)$ the cumulative probability of fibers broken within the effective pullout length when the bridging fiber stress is T. Then, σ is given by

$$\frac{\sigma}{V_f} = T\left\{1 - \frac{1}{2}\left(\frac{T}{\sigma_c}\right)^{m+1}\right\} \quad (15)$$

where m is a Weibull modulus obtained in single fiber tension tests, and σ_c is a representative strength at the gage length of $2l_f$. Then, calculating the maximum value of T, the composite ultimate tensile strength σ_{UTS} is given by

$$\sigma_{UTS} = V_f \sigma_c \left(\frac{2}{m+2}\right)^{1/(m+1)}\left(\frac{m+1}{m+2}\right) \quad (16)$$

3.5. Average strain

If all matrix crack spacings are assumed to be equal, the strain between two matrix cracks are equal to the average strain in the composite. Considering both bonded and debonded regions, the average strain ε in the composite is given by

$$\varepsilon = \varepsilon_f^+ + 2\left(\int_0^l \Delta\varepsilon_f\, dz\right)\Big/ d \quad (17)$$

4. Experimental results

4.1. Composite tensile tests

The stress-strain curves for two types of composites are shown in Fig. 5. Composites with uncoated fibers are very brittle without debonding at the tips of matrix cracks and exhibit a linear stress-strain curve up to the final fracture. Composites with BN-coated fibers, on the other hand, show a linear stress-strain curve up to about 200 MPa and becomes quite nonlinear. The composite ultimate strength and strain are much higher for composites with BN-coated fibers than those with uncoated fibers. The weak interface as introduced by BN coating is necessary for the improvement of the composite strength properties.

4.2. Matrix cracking behavior

The densities of the matrix cracks measured through the replica observation are plotted in Fig. 6 along with the corresponding stress-strain curve for composites with BN-coated fibers. The observed matrix cracks are shown in Fig. 7. An initial matrix crack was observed at 192 MPa, which is close to the knee point where nonlinearity appears in the stress-strain curve. The density of matrix cracks kept increasing as the applied stress increased, and was saturated at about 270–300 MPa. The average crack spacing at the saturation was approximately 157 μm.

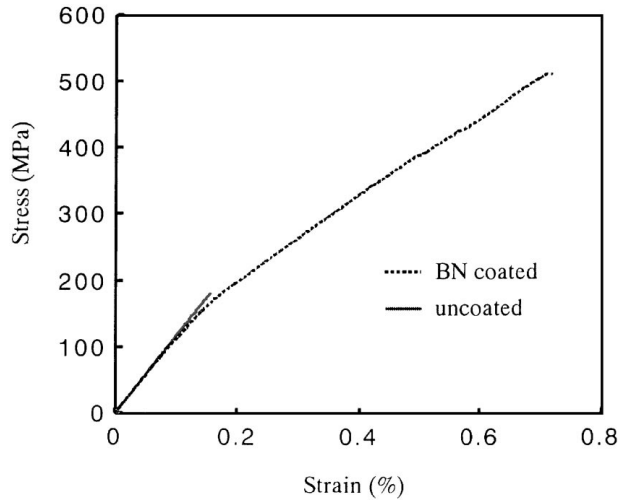

Figure 5 Stress-strain curves for composites reinforced with BN-coated and uncoated fibers.

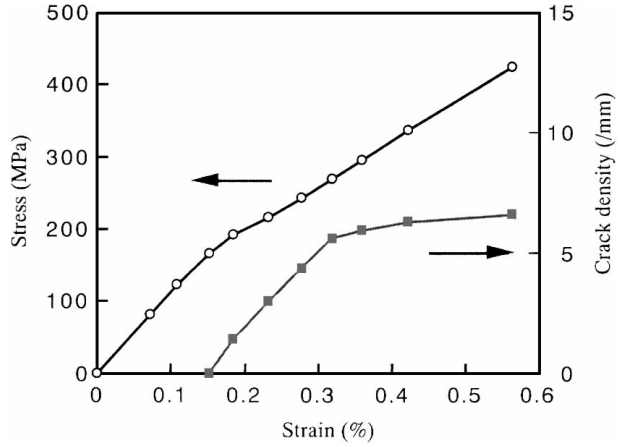

Figure 6 Experimental results of stress-strain curves and crack density.

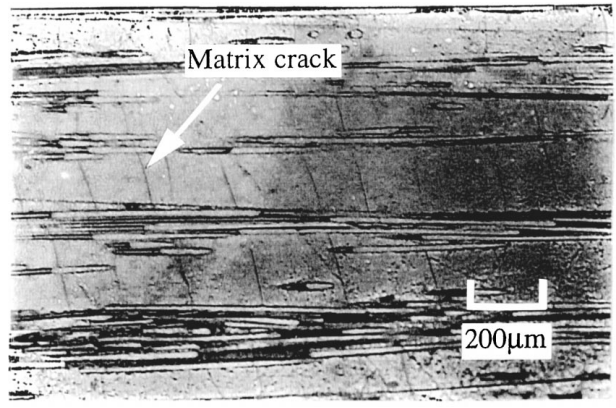

Figure 7 Photographs of matrix cracks.

TABLE II Mechanical properties of extracted HI-NICALON SiC fibers

Fiber statistical properties	Values
Mean strength	2.4 GPa
Minimum strength	1.6 GPa
Maximum strength	3.4 GPa
Shape parameter, m	4.0
Scale parameter, σ_0	2.7 GPa

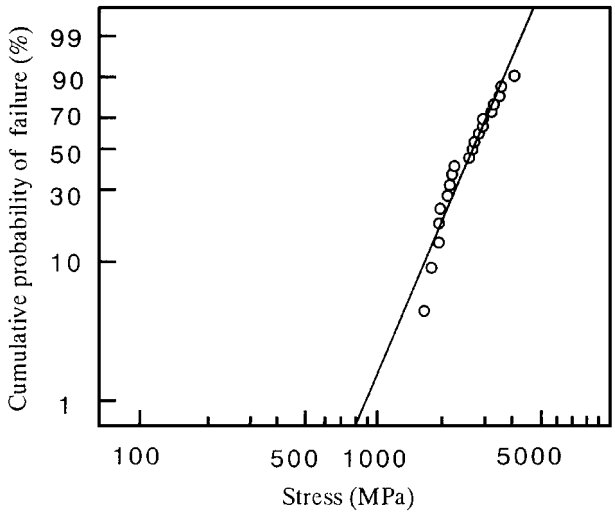

Figure 8 Strength distribution of extracted HI-NICALON SiC fibers.

4.3. Fiber strength tests

The fiber strength distributions of extrated fibers from the composites are shown in Fig. 8. The strength properties and the Weibull modulus are listed in Table II. The mean strength of virgin HI-NICALON^{TM} is almost 2.8 MPa, which is higher than that of the extrated fibers. No clear fracture mirrors were not observed on fracture surfaces of pull-out HI-NICALON fibers.

5. Discussion

5.1. Probabilistic prediction of average matrix crack density

The average matrix crack density predicted by Equation 11 is shown in Fig. 9. The mechanical data of the composites used for the prediction are listed in Table III. Here the scale parameter and the Weibull modulus of the matrix ($\sigma_{m0} = 44$ MPa, $\overline{m} = 1.34$) were obtained from the replica observation results using Equation 10. However, since these data are calculated from the experimental data, it should be noted that they may not be the intrinsic fracture strength of matrix itself. The prediction agrees well with the experimental data. The model proposed by Vagaggani *et al.* [8] does not exactly fit the experimental data due to the assumption that no matrix cracks are generated after a certain saturation point. In fact, a few cracks are generated after they tend to be saturated.

5.2. Determination of interfacial properties

The debonding length l predicted by Equation 13 with changing g_{ic} is shown in Fig. 10. Here the interfacial

TABLE III Mechanical properties of consituent materials

Material properties	Values
Fiber modulus with BN coating, E_f	230 GPa
Matrix modulus, E_m	60 GPa
Fiber volume fraction, V_f	0.31
Fiber radius, R_f	8 μm
Poisson's ratio, $\nu_f = \nu_m$	0.2
Fiber thermal expansion coefficient, α_f	3.10×10^{-6}
Matrix thermal expansion coefficient, α_m	3.25×10^{-6}
Temperature change, ΔT	-1000 °C

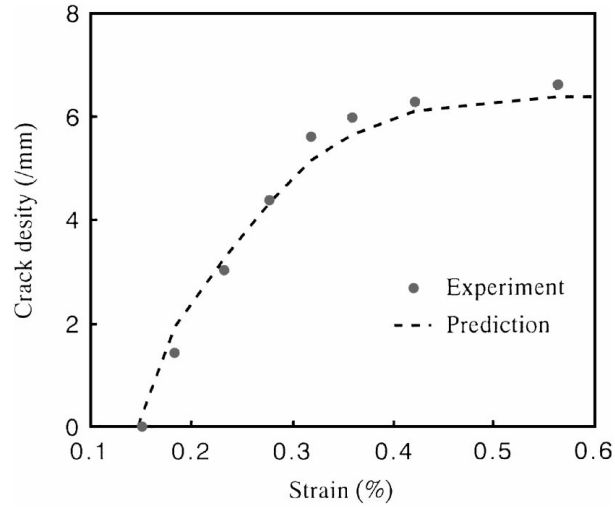

Figure 9 Comparison between predicted and experimental crack densities.

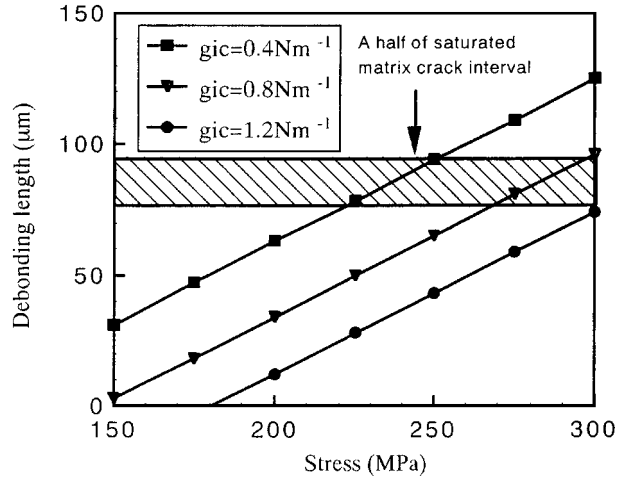

Figure 10 Predicted debonding length with changing g_{ic} ($\tau = 7.6$ MPa).

sliding stress τ can be estimated by the multiple fracture method [10, 12] using the average matrix crack spacing at saturation d_s and given by

$$\tau = 1.34 \left\{ \frac{\Gamma_m R_f^2 E_m E_f V_m^2}{E_c V_f d_s^3} \right\}^{1/2} \quad (18)$$

where Γ_m is the fracture energy of matrix. The calculated τ value for composites with BN-coated fibers is 7.6 MPa. The shaded region in Fig. 10 corresponds to the range in a half of the saturated matrix crack spacing. The Hutchinson and Jensen model does not have any stress recovery region of the matrix in the bonding

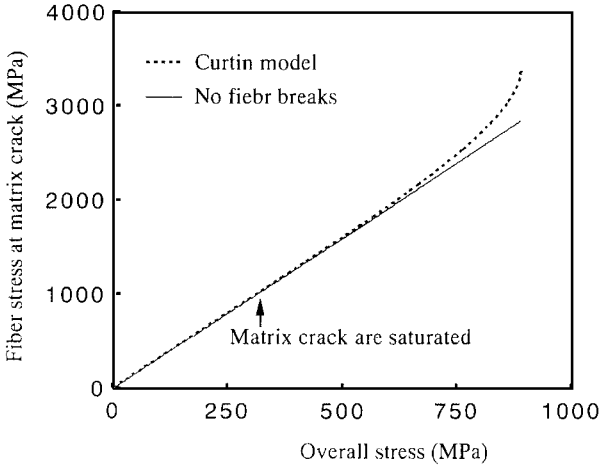

Figure 11 Axial fiber stress at the matrix crack plane.

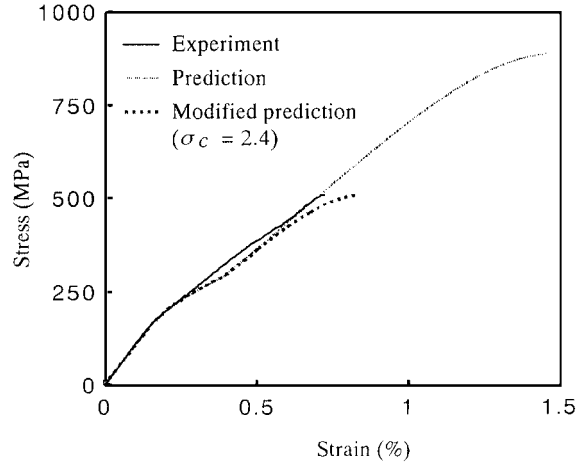

Figure 12 Comparison between predicted and experimental stress-strain curves.

region. Therefore, if we assume the matrix crack saturation occurs when the neighboring debondings connect with each other, matrix cracks are saturated when debonding length reaches the shaded region. Since matrix cracks are saturated at about 270–300 MPa, the appropriate value for g_{ic} is found to be approximately 0.8 N m^{-1}.

5.3. Fiber stress at a matrix crack plane

The fiber stress T calculated from the applied stress σ by Equation 15 is shown in Fig. 11. If no fiber breaks occur, T is equal to σ/V_f, which is also shown in Fig. 11. The arrow in Fig. 11 denotes the stress where matrix cracks are saturated (270–300 MPa). The difference of two curves is very small until 600 MPa, but becomes gradually larger as the applied stress increase, because some fibers begin to break. The Curtin model has been developed only in the strain range after the matrix cracks are saturated. However, the Curtin model can be appropriately used in the stress range where only a few fibers break.

5.4. Prediction of stress-strain curves

The predicted stress-strain curve is shown in Fig. 12. Here, to compare with experimental strain obtained from strain gauge, effective strain ε_{eff} was used and is given by

$$\varepsilon_{eff} = \varepsilon - a_6\varepsilon_z^T \tag{19}$$

This analysis used the strength data of fibers extracted from the composites as shown in Table II, and $\tau =$ 7.6 MPa. Predicted and experimental stress-strain curves are similar until 400 MPa. However σ_{UTS} predicted by the Curtin model normally provides the ideal composite ultimate tensile strength, which is larger than the experimentally-obtained tensile strength (512 MPa).

This is because the strength data of extracted fibers exceed those in real composites. Although the experimental strength data of fibers (NICALON) [13] ($\sigma_0 = 1.8$ MPa) used by Curtin is much lower than our experimental data (shown in Table I), the composite with those weaker fibers has almost the same ultimate tensile strength as our experimental results. Using the strength data of fibers ($\sigma_c = 2.4$ MPa) calculated from experimental σ_{UTS} (512 MPa), the modified stress-strain curve is also shown in Fig. 12. This results are similar to experimental results. Thus, the strength data of fibers in real composites are found to be very important factor to predict the stress-strain curve and ultimate tensile strength. Further investigation is necessary to establish the way how the strength of HI-NICALON^{TM} are estimated.

Fracture surfaces observed with SEM after the tensile failure are shown in Fig. 13. Fiber pull-outs can be found in fiber-rich regions more frequently than in matrix-rich regions. It is considered that an initial matrix crack generated in a matrix-rich region tends to propagate in a brittle manner and decreases the composite tensile strength. The composite ultimate tensile strength can be increased by the reduction in local scatter of fiber spacial distribution in the cross-section as well as by improvement of the specimen configuration.

The stress-strain curve predicted for SiC (NICALON)/CAS [14] is shown in Fig. 14. The mechanical data of the composites are listed in Table IV. It should be noted that the strength data of fibers is obtained from another paper [15]. They observed the fracture mirror of the broken fibers and obtained *in situ* fiber strength parameters $\sigma_c = 2.0$ MPa and $m = 2$. The prediction has a good agreement with the experimental results.

TABLE IV Mechanical properties of CAS/NICALON composites

Material properties	Values
Fiber modulus with BN coating, E_f	195 GPa
Matrix modulus, E_m	98 GPa
Fiber volume fraction, V_f	0.35
Fiber radius, R_f	7.5 μm
Poisson's ratio, $\nu_f = \nu_m$	0.2
Fiber thermal expansion coefficient, α_f	4.0×10^{-6}
Matrix thermal expansion coefficient, α_m	5.0×10^{-6}
Temperature change, ΔT	-1000 °C
Sliding stress, τ	12 MPa
Interface toughness, g_{ic}	2.5 N m^{-1}

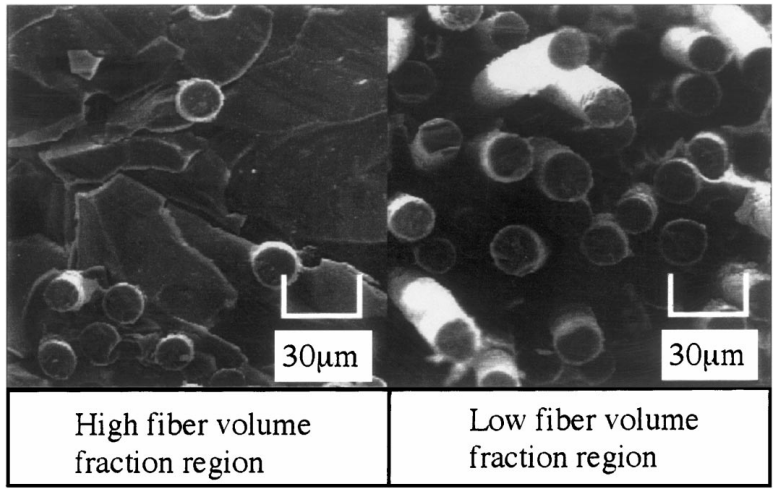

Figure 13 Photographs of fracture surfaces.

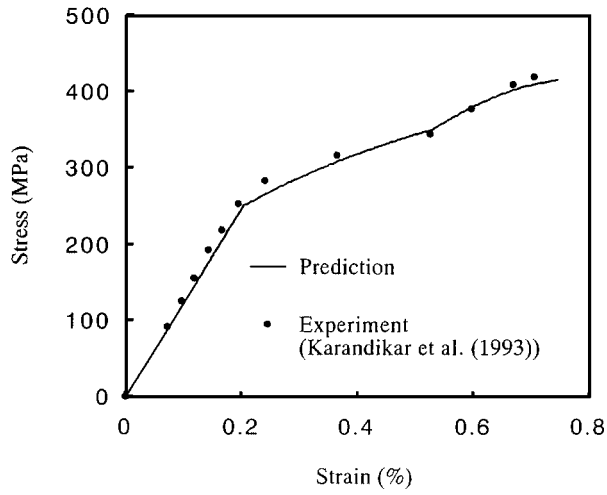

Figure 14 Comparison between predicted and experimental stress-strain curves (CAS/NICALON).

The present model is applicable to the other materials which have the same damage process. In addition, when the experimental stress-strain curve is obtained, the present model is useful for obtaining micro-mechanical properties and optimazing the material design.

6. Conclusions

The tensile damage initiation and growth behavior in BN-coated HI-NICALON SiC fiber reinforced glass matrix composites was experimentally clarified by replica observations. The improved axisymmetric cylindrical model was used to predict the stress-strain behavior, and the following conclusions were obtained: The improved axisymmetric cylindrical models with two matrix cracks predicted the stress-strain curve reasonably well. The prediction of ultimate tensile strength considering the fiber strength distribution of the extracted fibers provided a larger value than the experimental data, but the difference is expected to be decreased by establishing the way to exactly measure the strength data of fibers in real composites (such as single fiber composite tests), reducing in local scatter of fiber spacial distribution in the cross-section and improvement of the specimen configuration.

Acknowledgement

We thank Professor Curtin for his useful advice concerning the theoretical analysis especially on the ultimate tensile strength, and Mr. M. Yanaka and Miss A. Nakai for fruitful discussions.

References

1. K. M. PREWO and J. J. BRENNAN, *J. Mater. Sci.* **15** (1980) 463–468.
2. D. B. MARSHALL and A. G. EVANS, *J. Amer. Ceram. Soc.* **68** (1985) 225–231.
3. D. C. CRANMER, *Amer. Ceram. Soc. Bull.* **68** (1989) 415–419.
4. L. S. SIGL and A. G. EVANS, *Mech. Mater.* **8** (1989) 1–12.
5. J. W. HUTCHINSON and H. M. JENSEN, *ibid.* **9** (1990) 139–163.
6. D. B. MARSHALL, *Acta Metall. Mater.* **40** (1992) 427–441.
7. D. B. MARSHALL and W. C. OLIVER, *J. Amer. Ceram. Soc.* **70** (1987) 542–548.
8. E. VAGAGGINI, J. M. DOMERGUE and A. G. EVANS, *ibid.* **78** (1995) 745–755.
9. H. CAO and M. D. THOULESS, *ibid.* **73** (1990) 2091–2094.
10. W. A. CURTIN, *ibid.* **74** (1991) 2837–2845.
11. N. TAKEDA and M. KIRIYAMA, *Composites Part A* **30** (1999) 593.
12. J. AVESTON, G. A. COOPER and A. KELLY, The Properties of Fiber Composites, Conf. Proc. Nat. Phys. Lab., Guildford (IPC Sci. Tech., Teddington, UK, 1971) pp. 15–26.
13. K. PREWO, *J. Mater. Sci.* **21** (1980) 463–468.
14. P. KARANDIKAR and T. W. CHOU, *Comp. Sci. Technol.* **74** (1993) 2837–2845.
15. D. S. BEYERLE, S. M. SPEARING, F. W. ZOK and A. G. EVANS, *J. Amer. Ceram. Soc.* **75** (1992) 2719–2725.

Received 24 August 1998
and accepted 13 January 1999